Characterization and Comparative Analysis of Structural, Optical and Gas-Sensing Properties of Aluminum-Doped Titanium Dioxide Thin Films

Reem Sami Ali[1], Hiba Saad Rasheed[2], Huda Saadi Ali[3], Wathiq Ayoub Taha Al Ramdhan[4] and Hassan Hadi Darwoysh[2]

[1]*Department of Physics, College of Science, Mustansiriyah University, 10052 Baghdad, Iraq*
[2]*Department of Physics, College of Education, Mustansiriyah University, 10052 Baghdad, Iraq*
[3]*Department of Renewable Energy, College of Energy and Environmental Sciences, Al-Karkh University of Science, 10003 Baghdad, Iraq*
[4]*Department of Medical Physics, Al-Manara College for Medical Sciences, 62001 Amarah, Maysan, Iraq*
hassan.hadi66@uomustansiriyah.edu.iq

Keywords: TiO_2, Al Doping, CSP, Nanostructured Thin Films, Gas Sensing.

Abstract: This study examined some physical characterizations of aluminum-doped TiO_2 (TiO_2:Al) nanostructured thin films. Films with 0%, 2%, and 4% Al were deposited via chemical spray pyrolysis (CSP). A polycrystalline tetragonal anatase phase with preferred orientation along the (101) plane was verified by X-ray diffraction. Al^{3+} incorporation enhanced crystallinity, increasing crystallite size from 17.52 nm to 32.38 nm while reducing dislocation density and lattice strain. Atomic force microscopy revealed uniform nanoscale grains, with both particle size and surface roughness decreasing as Al content increased, indicating dopant-induced modifications in nucleation and growth. UV-Vis spectroscopy showed moderate transparency and a reduction in the direct optical band gap from 3.44 eV for undoped TiO_2 to 3.32 eV for 4% Al-doped films, attributed to defect states introduced by Al doping. Higher Al concentration increased electrical resistance but decreased sensitivity in gas-sensing studies toward NO_2 at 140°C, most probably as a result of changed surface adsorption and reduced charge-carrier mobility. Overall, Al doping tunes structural and optical properties effectively, though optimizing the dopant concentration is essential to balance material enhancements with functional gas-sensing performance.

1 INTRODUCTION

TiO_2 is a widely studied material with extensive utilization across diverse fields [1]-[3]. Its utility stems from its high transparency in the visible spectrum combined with a relatively high average refractive index [4]. Moreover, TiO_2 exhibits notable photochromic behavior, making it a material of interest for optical and photonic applications [5]. The intrinsic absorption threshold of titanium dioxide at the blue edge of the visible spectrum, together with its thermodynamic stability, non-toxicity, and cost-effective synthesis of dispersed TiO_2, renders it highly suitable for applications as both a white pigment and a photocatalyst [6], [7]. Chemical reactions involving aluminum and appropriate metal oxides, such as CuO [8], Fe_2O_3 [9], and TiO_2 [10], [11], were widely utilized. These methods leverage the principle that aluminum can reduce these oxides, generating a different metal alongside aluminum oxide. The metal produced can serve as a beneficial alloying component for the aluminum matrix or can form intermetallic compounds with aluminum that act as reinforcements. Notably, aluminum oxide, particularly Al_2O_3, serves as an effective reinforcement for AMCs [12]. Among the various reactive pairs involving aluminum and metal oxides, the Al-TiO_2 system stands out for its Al_3Ti. At both room temperature and higher temperatures, one of its derivative forms has good mechanical properties [13], [14]. Gas sensors based on titanium dioxide (TiO_2) have been shown to have a high sensitivity and stability under harsh environmental conditions, highlighting their potential as the preferred material for high-temperature gas sensing applications [15]-[17]. TiO_2 exists in three distinct crystalline phases: rutile, anatase, and brookite. Among the three crystalline forms, anatase and rutile are the most commonly observed, as brookite is relatively unstable [18]. The specific phase of TiO_2 significantly affects its properties, including catalytic activity and gas-sensing performance [19]. In particular, the anatase phase is often favored, especially in reducing environments such as carbon monoxide (CO) detection [20]. Enhancing the surface area of TiO_2 can further improve sensor sensitivity by increasing the number of available surface oxygen sites for gas interactions. Consequently, nanoscale TiO_2, characterized by a high surface-to-weight ratio, is expected to exhibit superior sensitivity in TiO_2-based gas sensors [21], [22]. In this study, aluminum-doped TiO_2 nanostructured thin films were synthesized using CSP, which enables the fabrication of homogeneous coatings over large areas [23], [24]. In this work, we investigate the impact of Al doping on some physical characteristics and gas-sensing properties of TiO_2 nanostructured thin films. Various Al concentrations were used to systematically investigate their effects on crystal structure, surface morphology, optical characteristics, and sensing performance. Understanding these effects is vital to optimizing TiO_2-based materials for potential applications in gas sensor technologies.

2 EXPERIMENTAL

Undoped TiO_2 and aluminum-doped TiO_2 films were deposited via CSP method. 0.1 M of $TiCl_4 \cdot 5H_2O$ was prepared in deionized water, and aluminum, obtained from Sigma-Aldrich (Germany), was used as the doping agent. The solution was mixed with two or three drops of HCl to achieve complete clarity. The deposition was carried out with glass substrate maintained at 400 °C, and the spray nozzle positioned 28 cm from the base surface. The spray rate was set to 4 mL/min and the spraying time was 10 s, followed by a 90 seconds wait to prevent substrate cooling. The carrier gas used was nitrogen. The film thickness was measured by weighing and found to be 320 ±30 nm. AFM was used to examine surface morphology, while XRD was employed to determine crystal structure. Optical transmittance measurements were done via a double-beam Shimadzu UV-VIS spectrophotometer. Gas-sensing measurements were conducted in a cylindrical chamber with a radius of 7 cm and a height of 17 cm.

3 RESULTS AND DISCUSSION

Figure 1 presents the X-ray diffraction (XRD) patterns of the deposited films. The diffraction patterns exhibit characteristic peaks at 25.22°, 37.85°, 53.63°, and 62.67°, corresponding to the (101), (004), (105), and (220) crystallographic planes of anatase TiO_2, respectively. The strongest diffraction peak is observed for the (101) plane, indicating the preferential orientation of the crystallites along this direction. These diffraction peaks are in good agreement with ICDD card No. 21-1272, confirming the formation of the anatase crystalline phase. The sharp and well-defined diffraction peaks indicate good crystallinity of the deposited films. Furthermore, the absence of additional diffraction peaks associated with secondary phases or aluminum-containing compounds suggests that Al ions were successfully incorporated into the TiO_2 lattice rather than forming separate phases.

The crystallite size was estimated using the Scherrer method [25], [26], and the calculated values are summarized in Table 1. The crystallite size increased from 17.52 to 32.38 nm with increasing aluminum dopant concentration. This increase indicates enhanced crystal growth and improved crystallinity, which may be attributed to the promotion of grain growth and the reduction of lattice imperfections during film formation.

The dislocation density was calculated from the crystallite size [27], [28]. As shown in Table 1, the dislocation density decreased from 39.56 to 25.27 with increasing aluminum concentration, indicating an improvement in crystal quality due to the reduction of structural defects within the crystal lattice.

The lattice strain was also determined from the XRD peak broadening [29], [30]. As presented in Table 1, the strain decreased from 29.79 to 20.14 as the aluminum dopant concentration increased, suggesting relaxation of internal lattice stresses and improved structural ordering. Figure 2 illustrates the variation of the structural parameters, including crystallite size, dislocation density, lattice strain, and full width at half maximum (FWHM), while Table 1 summarizes the corresponding FWHM values used in the structural analysis.

Figure 3 presents the atomic force microscopy (AFM) images of TiO_2 and Al-doped TiO_2 thin films. The surface morphology shows nanoscale grains uniformly distributed across the films, confirming the formation of nanostructured layers. The average particle sizes P_{av} were determined to be 84.1 nm, 67.8 nm, and 46.2 nm for undoped TiO_2, TiO_2:2% Al, and TiO_2:4% Al, respectively, while the corresponding root mean square (RMS) roughness values were 9.23 nm, 6.05 nm, and 4.67 nm. The average surface roughness (Ra) decreased from 7.37 nm to 3.65 nm with increasing Al content. This increment in particle size and surface roughness is attributed to the effect of Al ions on nucleation and growth, resulting in a more compact, uniform film surface. The AFM parameters A_{para}, including particle size, Ra, and RMS roughness, are summarized in Table 2, highlighting the significant role of Al doping in enhancing surface morphology.

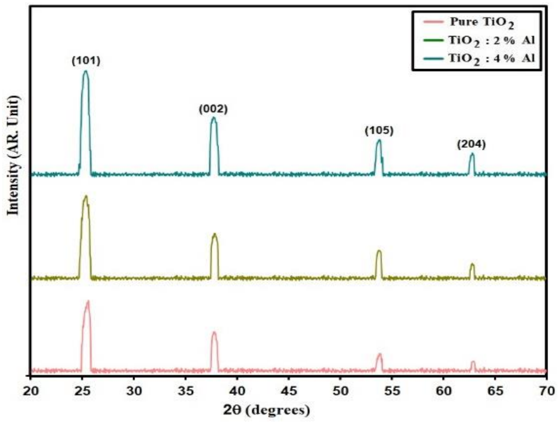

Figure 1: XRD patterns of undoped and Al-doped TiO_2 thin films.

Figure 4 shows the variation of transmittance (T); The findings show that the films have an average amount of optical transparency in the visible spectrum, with transmittance values ranging from 74.3% to 78.1%. Furthermore, the transmittance increases gradually with the longer wavelength. This increase in transmittance at higher wavelengths indicates reduced light absorption in the near-infrared region, mainly due to lower photon energy, which is insufficient to excite electrons across the band gap. Such behavior is typical of wide-band-gap semiconductor materials like TiO_2, where absorption is stronger in the ultraviolet and decreases toward the visible and infrared regions [31], [32].

The absorbance (A) of the films was determined from the transmittance (T), based on the incident light intensity (I_0) and the transmitted light intensity (I) [33], [34].

As illustrated in Figure 5, the pure TiO_2 film exhibits the lowest absorbance, whereas the TiO_2 films doped with 2% and 4% aluminum display progressively higher absorbance values. This increase in absorbance can be assigned to the incorporation of Al into the TiO_2 lattice, which introduces additional defect states and impurity energy levels within the band gap. These localized states enhance the probability of electronic transitions and facilitate the absorption of incident photons [35], [36].

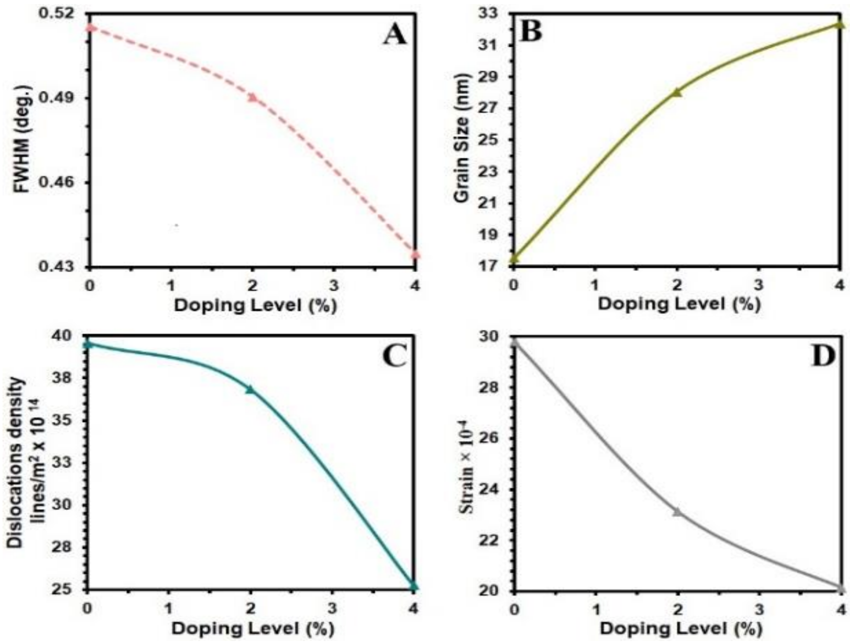

Figure 2: Variation of the structural parameters of undoped and Al-doped TiO_2 thin films.

Table 1: Structural parameters and optical band gap of undoped and Al-doped TiO_2 thin films.

Specimen	(hkl) Plane	2 θ (°)	FWHM (°)	E_g (eV)	D (nm)	δ (× 10^{14}) (lines/m^2)	ε (× 10^{-4})
Undoped TiO_2	101	25.23	0.52	3.44	17.52	39.56	29.79
TiO_2: 2% Al	101	25.20	0.49	3.38	28.67	36.82	23.12
TiO_2: 4% Al	101	25.16	0.44	3.32	32.38	25.27	20.14

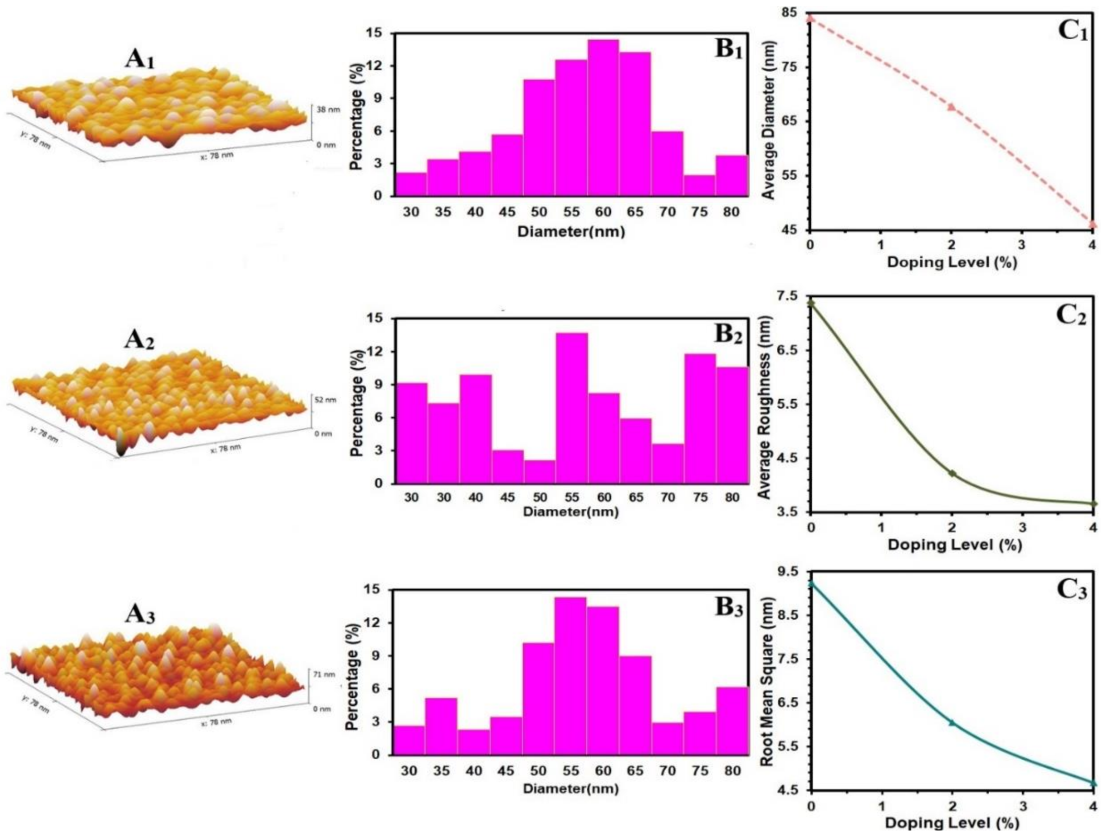

Figure 3: AFM surface images of undoped and Al-doped TiO_2 thin films.

Table 2: AFM surface morphology parameters of undoped and Al-doped TiO_2 thin films.

Sample	P_{av} nm	Ra (nm)	rms (nm)
TiO_2	46.2	3.65	4.67
TiO_2: 2% Al	67.8	4.22	6.06
TiO_2: 4% Al	84.1	7.37	9.23

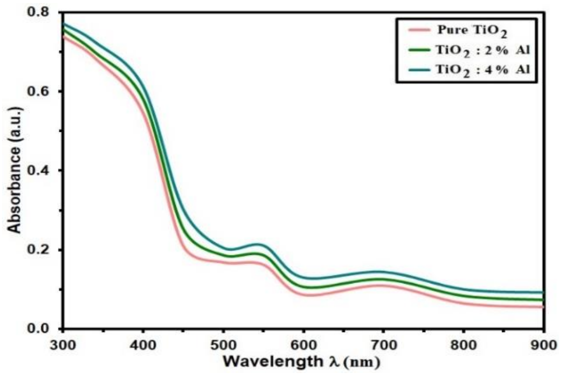

Figure 4: Optical transmittance spectra of undoped and Al-doped TiO_2 thin films.

The absorption coefficient (α) of the films was calculated from the absorbance and film thickness (t) [37].

Figure 6 illustrates the variation of α with photon energy (hν) for undoped and Al-doped TiO_2 thin films. The results indicate that α increases with higher aluminum doping concentrations, particularly near the absorption edge, where a sharp rise reflects strong optical absorption due to electronic transitions from the valence band (VB) to the conduction band (CB). At higher photon energies, α gradually decreases. The absorption coefficient reaches values on the order of 10^4 cm^{-1}, confirming pronounced optical absorption and suggesting dominant direct electronic transitions within the band structure. The enhancement of α with Al doping is attributed to modifications in the electronic structure, in which Al incorporation introduces additional defect states and localized energy levels within the band gap, thereby improving the films' photon-absorption capability [38], [39].

The films' direct band gap (Eg) was calculated using the Tauc relation between the absorption coefficient and photon energy, with n = 1/2 corresponding to allowed direct transitions [40], [41].

As shown in Figure 7, Eg of TiO_2 thin films diminishes with rising aluminum doping concentration. This reduction is credited to the creation of defect states and impurity levels within Eg caused by Al incorporation, which introduces additional energy levels between VB and CB, enabling electronic transitions at lower hν. Consequently, Eg narrows from 3.44 eV for undoped TiO_2 to approximately 3.32 eV for the highest Al-doped films. Increased structural disorder and defect density due to Al doping further contribute to band tailing and effective band gap narrowing [42], [43].

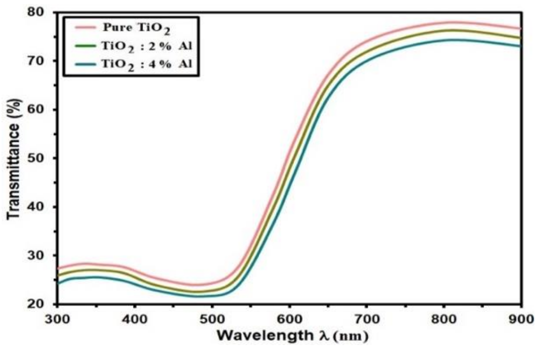

Figure 5: Optical absorbance spectra of undoped and Al-doped TiO_2 thin films.

The extinction coefficient (k) was evaluated from the absorption coefficient (α) and wavelength (λ) [44], [45].

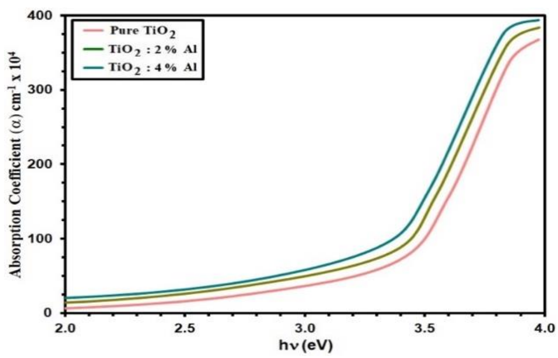

Figure 6: Absorption coefficient (α) as a function of photon energy (hν) for undoped and Al-doped TiO_2 thin films.

Figure 8 shows the variation of k with λ. The results indicate that k increases rapidly in the ultraviolet (UV) region and then gradually decreases with increasing wavelength. This behavior is related to the material's optical absorption properties. The nonzero values of k below the fundamental absorption edge indicate sub-band-gap absorption, which is mainly attributed to defect states, impurity levels, and localized energy states within the band gap caused by structural imperfections or dopant incorporation [46].

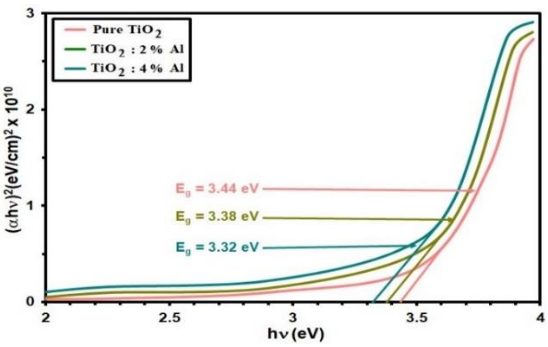

Figure 7: Tauc plots for determining the optical band gap (Eg) of undoped and Al-doped TiO_2 thin films.

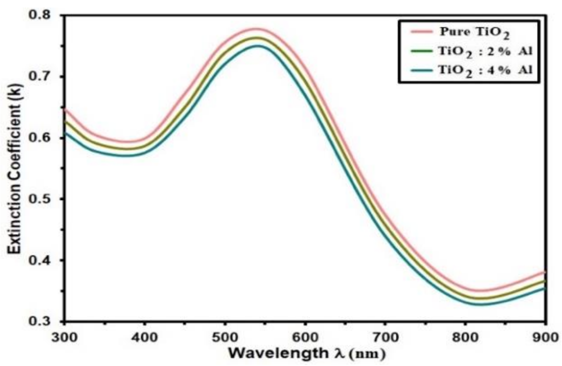

Figure 8: Extinction coefficient (k) spectra of undoped and Al-doped TiO_2 thin films.

The refractive index (n), which describes the propagation of light within the material, was determined from the reflectance (R) and extinction coefficient (k) [47], [48].

Figure 9 shows n of TiO_2 thin films as a function of λ. For all Al-doped films, n increases with wavelength but decreases with higher Al content. This reduction is attributed to changes in electronic polarizability and structural modifications caused by Al incorporation, including lattice distortions and reduced film density [49], [50], [59].

The gas-sensing performance was evaluated at 140 °C, and Figure 10 shows the resistance variation of the TiO_2 films exposed to 225 ppm NO_2. Undoped TiO_2 exhibited the lowest resistance, indicating efficient NO_2 adsorption and high charge carrier mobility [51], [52]. In contrast, TiO_2 doped with 4% Al showed the highest resistance, likely due to dopant-induced modifications in the electronic structure that hinder charge transport and alter surface interactions with NO_2 molecules. These results demonstrate that Al doping increases the resistance and significantly affects the gas-sensing behavior of TiO_2 films [53], [54].

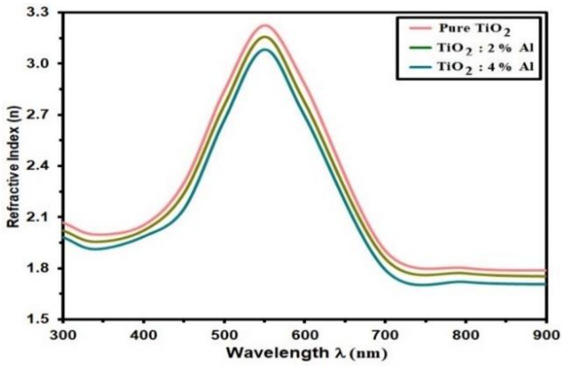

Figure 9: Refractive index (n) spectra of undoped and Al-doped TiO_2 thin films.

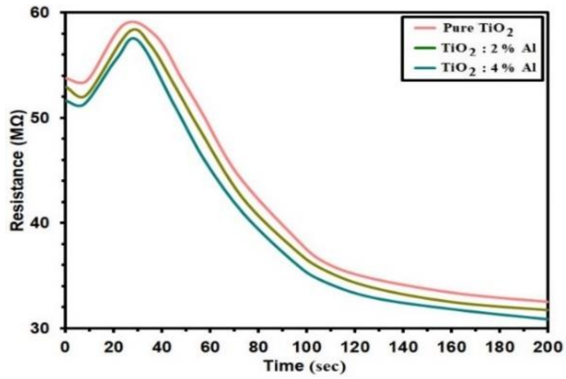

Figure 10: Resistance response of undoped and Al-doped TiO_2 thin films to 225 ppm NO_2 at 140 °C.

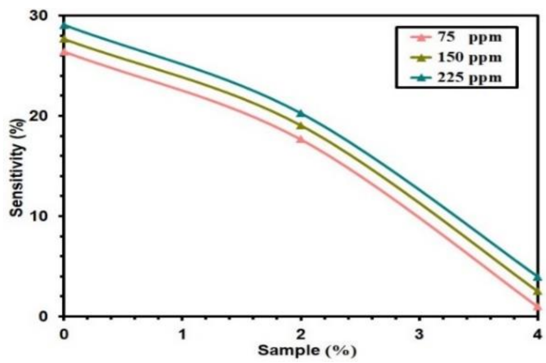

Figure 11: Gas sensitivity of undoped and Al-doped TiO_2 thin films toward NO_2.

The sensitivity (S) was calculated from the relative change in resistance between air and gas exposure, where Rg and Ra represent the resistance of the film sensor in the presence of gas and in air, respectively [55].

Figure 11 shows S of TiO_2, TiO_2:2% Al, and TiO_2:4% Al thin films toward NO_2 gas. The results show that sensitivity decreases with increasing Al doping, reflecting enhanced carrier recombination and reduced sensor response. Specifically, at 75, 150, and 225 ppm NO_2, the sensitivity drops from 26.42% to 1.01%, 27.65% to 2.52%, and 29.06% to 3.96%, respectively. This decline is attributed to dopant-induced structural modifications that hinder charge-carrier mobility, thereby diminishing the films' gas-sensing performance [56]-[58].

4 CONCLUSIONS

Aluminum-doped TiO_2 nanostructured films were successfully created via chemical spray pyrolysis. The structural analysis verified a single-phase anatase structure in all films, signifying substitutional incorporation of Al^{3+} ions into the TiO_2 lattice. This incorporation significantly influenced the microstructural properties: crystallite size rose, while both dislocation density and lattice strain rose with higher Al content, indicating improved overall crystalline quality. Morphologically, Al doping led to a smoother, more compact surface, as both the average particle size and surface roughness were increased. Optically, the films remained highly transparent. The decrease in Eg with rising Al content is a key finding, proposing that doping can be used to tailor the light absorption edge of TiO_2 for specific optoelectronic applications. However, the gas-sensing results for NO_2 revealed a complex trade-off. While Al doping increased the films' baseline resistance, it concurrently reduced their sensitivity.

ACKNOWLEDGMENTS

The authors thank Mustansiriyah University (www.uomustansiriyah.edu.iq) for providing the tools and support required to complete this study.

REFERENCES

[1] K. Nagaraj, S. Radha, C. G. Deepa, K. Raja, V. Umapathy, N. P. Badgujar, and C. Uthra, “Photocatalytic advancements and applications of titanium dioxide (TiO_2): Progress in biomedical, environmental, and energy sustainability,” Next Research, vol. 2, no. 1, 100180, 2025.

[2] H. Nosrati and M. Heydari, “Titanium dioxide nanoparticles: a promising candidate for wound healing applications,” Burns & Trauma, vol. 13, tkae069, 2025.

[3] N. Parveen, S. A. Ansari, K. M. Alnahdi, H. H. Hammud, W. A. Aljamhi, M. W. Alam, and

[4] W. Al Zoubi, “Eco-friendly synthesis and applications of graphene-titanium dioxide nanocomposites for pollutant degradation and energy storage,” J. Photochem. Photobiol. A: Chem., vol. 459, 116096, 2025.

[5] Y. Liu, D. Wang, J. Zhang, Y. Wang, X. Yu, J. Chen, and Y. Takeoka, “Synthesis and UV-Curing Mechanism of High-Refractive-Index Transparent Nanocomposites Embedded with Surface-Engineered TiO2 Nanoparticles,” Composites Part B: Engineering, 113116, 2025.

[6] A. V. Khlyustova, A. V. Evdokimova, V. D. Shibaeva, and N. A. Sirotkin, “Photochromic properties of TiO2: doping effect,” Bull. Russ. Acad. Sci.: Phys., vol. 89, no. 10, pp. 1889-1895, 2025.

[7] Z. Zhang, Z. Ma, Z. Du, Y. Chen, Q. Zhang, H. Du, and M. Zendehdel, “Self-Assembly in Thin-Film Photovoltaics: Advancing Energy Conversion through Tailored,” in Functional Nanostructures for Energy Conversion and Advanced Applications, p. 61, 2026.

[8] P. Ramu and D. Patil, “Titanium dioxide coating for biomedical,” in High-Performance Metallic Biomaterials: Surface Modification and Coating of Implants, vol. 15, p. 101, 2025.

[9] Abdallah, J. Zapata, G. Lahiner, B. Warot-Fonrose, J. Cure, Y. Chabal, and C. Rossi, “Structure and chemical characterization at the atomic level of reactions in Al/CuO multilayers,” ACS Appl. Energy Mater., vol. 1, no. 4, pp. 1762-1770, 2018.

[10] W. Zhang, B. Yin, R. Shen, J. Ye, J. A. Thomas, and Y. Chao, “Significantly enhanced energy output from 3D ordered macroporous structured Fe2O3/Al nanothermite film,” ACS Appl. Mater. Interfaces, vol. 5, no. 2, pp. 239-242, 2013.

[11] R. Agravat, S. K. Patel, A. K. U, T. Saidani, and A. Armghan, “Design of Metamaterial Surface Plasmon Resonance Solar Absorber Design Based on MXene-TiO2-Al Material for Renewable Energy Applications,” Plasmonics, vol. 20, no. 10, pp. 8689-8705, 2025.

[12] M. M. Mutter, R. H. Jabbar, and A. I. Khudiar, “Synthesis and characterization of TiO2: Al thin films for bacteria resistance in the implanted dental,” J. Aust. Ceram. Soc., vol. 58, no. 1, pp. 145-149, 2022.

[13] Q. Zhang, B. L. Xiao, W. G. Wang, and Z. Y. Ma, “Reactive mechanism and mechanical properties of in situ composites fabricated from an Al-TiO2 system by friction stir processing,” Acta Mater., vol. 60, no. 20, pp. 7090-7103, 2012.

[14] T. Li, E. Al Olevsky, and M. A. Meyers, “The development of residual stresses in Ti6Al4V-Al3Ti metal-intermetallic laminate (MIL) composites,” Mater. Sci. Eng. A, vol. 473, no. 1-2, pp. 49-57, 2008.

[15] Qin, S. Zhang, Z. Ma, and B. Lu, “Interfacial characteristics and mechanical properties of TiAl4822/Ti6Al4V metal-intermetallic laminate composite prepared through vacuum hot pressing,” Materials, vol. 18, no. 4, 898, 2025.

[16] W. Cheng, X. Li, C. Han, Y. Liu, A. Xue, H. Dong, and Y. Liu, “Room-Temperature Wearable Chemiresistor Based on a Flexible Inorganic Photoactive Anatase-Rutile TiO2/Yttria-Stabilized Zirconia Nanofiber Network,” ACS Sensors, vol. 10, no. 3, pp. 2125-2135, 2025.

[17] C. Zhang, T. Wang, G. Zhang, R. Gao, C. Gao, Z. Wang, and F. Xuan, “Rational Design and Fabrication of MEMS Gas Sensors With Long-Term Stability: A Comprehensive Review,” Adv. Sci., vol. 12, no. 39, e11555, 2025.

[18] A. M. Al Saleh, “A Review of the Synthesis, Structural, and Optical Properties of TiO2 Nanoparticles: Current State of the Art and Potential Applications,” Crystals, vol. 15, no. 11, 944, 2025.

[19] M. E. Morais, J. C. Z. Griz, R. Brackmann, R. D. C. da Rocha, and M. de Souza Sikora, “Hydrothermal tuning of anatase-brookite TiO_2 nanostructures: influence of synthesis parameters on surface charge, crystallite size, and photocatalytic activity,” Catal. Today, 115753, 2026.

[20] A. Devi, G. M. Reddy, M. Harsha, S. Sujith, S. P. Maradur, G. V. Shanbhag, and N. Nalajala, “Unravelling TiO2 phase-engineering for hydrogen (H2) gas sensor applications,” Mater. Sci. Eng. B, vol. 328, 119317, 2026.

[21] S. Singh, K. C. Stiwinter, J. P. Singh, and Y. Zhao, “Glancing Angle Deposition in Gas Sensing: Bridging Morphological Innovations and Sensor Performances,” Nanomaterials, vol. 15, no. 14, 1136, 2025.

[22] Y. Zhao, S. Guo, X. Feng, T. Xie, Z. He, and Y. Lin, “High-performance formaldehyde sensing of room-temperature UV-activated Mn-TiO2: Key effects of different crystal phase structures and Mn doping on carrier behavior and adsorption,” SSRN, [Online]. Available: https://ssrn.com/abstract=5702846.

[23] A. Trajcheva, P. Morales, J. Elgoyhen, and R. Tomovska, “Thiol-Functionalized TiO2 as Reactive Nanoadsorbents for Residual Monomer Removal from Waterborne Polymer Dispersions,” Ind. Eng. Chem. Res., 2026.

[24] H. H. Issa and B. A. Hasan, “Gas sensing characteristics of (TiO2)1−x(ZnO:MgO)x thin films doped and undoped with Au NPs for NO2 and H2S detection prepared by spray pyrolysis,” Appl. Phys. A, vol. 131, no. 12, 1026, 2025.

[25] K. Modhi and J. M. Rzaij, “Synthesis and characterization study of CuO thin film and CuO-CeO2 nanostructured composite using chemical spray pyrolysis,” in AIP Conf. Proc., vol. 2591, no. 1, p. 030066, 2023.

[26] A. A. Khadayeir, R. I. Jasim, S. H. Jumaah, N. F. Habubi, and S. S. Chiad, “Influence of substrate temperature on physical properties of nanostructured ZnS thin films,” Journal of Physics: Conference Series, vol. 1664, no. 1, 012009, 2020.

[27] A. Issa and K. A. Aadim, “Optical and structural characterization of ZnO:NiO nano composite prepared by pulsed laser deposition method,” J. Opt., vol. 54, pp. 2357-2362, 2025.

[28] B. Jumaa, T. H. Mubarak, and A. M. Mohammad, “Synthesis and characterization of spinel ferrite Co0.8Fe2.2O4 nanoparticle,” Journal of University of Anbar for Pure Science, vol. 15, no. 2, pp. 74-82, 2021.

[29] S. S. Chiad, H. A. Noor, O. M. Abdulmunem, N. F. Habubi, M. Jadan, and J. S. Addasi, “Optical and structural performance of nanostructured Te thin films by (CSP) with various thicknesses,” Journal of Ovonic Research, vol. 16, no. 1, pp. 35-40, 2020.

[30] S. Göktaş and G. Şahin, "Impact of different Cu sources on the structure, surface morphology, optical and photocatalytic characteristics of sol-gel derived CuO thin films," Türk Doğa ve Fen Derg., vol. 14, no. 1, pp. 13-20, 2025.

[31] S. S. Chiad, A. S. Alkelaby, and K. S. Sharba, "Optical conduct of nanostructure Co3O4 rich highly doping Co3O4: Zn alloys," Journal of Global Pharma Technology, vol. 11, no. 7, pp. 662-665, 2020.

[32] M. Tram, N. Nosidlak, M. M. Szindler, M. Szindler, K. Tokarczyk, P. Dulian, and J. Jaglarz, "Optical Studies of Al2O3:ZnO and Al2O3:TiO2 Bilayer Films in UV-VIS-NIR Spectral Range," Appl. Sci., vol. 15, no. 24, 12870, 2025.

[33] S. H. Mohamed and A. A. Alhazime, "Suppressing photoluminescence and enhancing light absorption of TiO2 via using TiO2/TiN/TiO2 plasmonic multilayers for better solar harvesting," J. Mater. Res. Technol., vol. 18, pp. 4470-4478, 2022.

[34] W. A. Aelawi, S. Alptekin, and M. H. Al-Timimi, "Structural, optical, and electrical properties of nanocrystalline CdS1−XCuSX thin films," Indian Journal of Physics, vol. 97, no. 13, pp. 3949-3956, 2023.

[35] M. A. Issa and K. A. Aadim, "Influence Of Laser Energy On Structural and Optical Properties of ZnO(x):NiO(1−x) Films Prepared By Pulse Laser Deposition," J. Opt., 2024.

[36] M. I. El-Henawey, M. Kubas, A. H. Oraby, A. El-Shaer, M. Abdelfatah, and H. Y. Salah, "Investigating the influence of Al2O3 doping on TiO2 optoelectronic properties and charge separation efficiency," Opt. Mater., vol. 156, 115955, 2024.

[37] M. M. Mohammed, A. Eid, M. N. El-Sheikh, O. A. Elkady, and A. Hassan, "Effect of CNTs addition on the Mechanical and Tribological Properties of Al-10 wt.% TiO_2 Nanocomposites Manufactured by Powder Metallurgy," Egypt. J. Chem., 2025.

[38] M. A. Issa and K. A. Aadim, "Study the structural and optical properties of Zinc Oxide prepared by pulse laser deposition," J. Opt., 2024.

[39] J. Leng, Y. Ding, M. Zhang, and J. Shen, "Effect of Indium Doping on the Photoelectric Properties of SnS Thin Films and SnS/TiO2 Heterojunctions," Coatings, vol. 15, no. 8, 972, 2025.

[40] M. M. El-Desoky, M. E. Abd-Elrazek, A. M. Elseman, and I. Morad, "Facile planetary ball mill synthesis, structural, photoluminescence, linear, and nonlinear optical features of Erbium-doped TiO2 nanoparticles," Appl. Phys. A, vol. 131, no. 5, 402, 2025.

[41] F. Habubi, K. H. Abass, S. S. Chiad, D. M. A. Latif, J. N. Nidhal, and A. I. Al Baidhany, "Dispersion parameters of polyvinyl alcohol films doped with Fe," Journal of Physics: Conference Series, vol. 1003, no. 1, 012094, 2018.

[42] A. A. Kamil, N. A. Bakr, T. H. Mubarak, and J. Al-Zanqanawee, "Effect of Au and Ag nanoparticles addition on the morphological, structural and optical properties of ZnO thin films deposited by sol-gel method," Journal of Ovonic Research, vol. 18, no. 3, pp. 431-442, 2022.

[43] G. C. Kaphle, R. P. Kharel, and B. P. Kafle, "Experimental and theoretical study on electronic and optical properties of TiO2 (anatase) bulk and Al doped thin film phases," J. Lumbini Eng. College, vol. 5, no. 1, pp. 17-27, 2023.

[44] C. C. Hsu, K. W. Huang, U. Kumar, Y. W. Suen, C. Sivakumar, and M. S. Ho, "Al-engineered anatase/rutile TiO2 heterostructures for superior resistive switching," Appl. Mater. Today, vol. 49, 103146, 2026.

[45] N. N. Jandow, N. F. Habubi, S. S. Chiad, I. A. Al-Baidhany, and M. A. Qaeed, "Annealing effects on band tail width, Urbach energy and optical parameters of Fe2O3:Ni thin films prepared by chemical spray pyrolysis technique," International Journal of Nanoelectronics and Materials, vol. 12, no. 1, pp. 1-10, 2019.

[46] A. A. Kamil, N. A. Bakr, T. H. Mubarak, and J. Al-Zanqanawee, "Synthesis and study of the optical and structural properties of Au and Ag nanoparticles by pulsed laser ablation (PLAL) technique," Digest Journal of Nanomaterials and Biostructures, vol. 16, no. 4, pp. 1219-1226, 2021.

[47] F. Yakuphanoglu and M. Arslan, "The fundamental absorption edge and optical constants of some charge transfer compounds," Opt. Mater., vol. 27, no. 1, pp. 29-37, 2004.

[48] A. A. Khadayeir, E. S. Hassan, T. H. Mubarak, S. S. Chiad, N. F. Habubi, M. O. Dawood, and I. A. Al-Baidhany, "The effect of substrate temperature on the physical properties of copper oxide films," Journal of Physics: Conference Series, vol. 1294, no. 2, 022009, 2019.

[49] M. I. Sayyed and S. Biradar, "Tuning optical properties and gamma-ray attenuation performance in PbO2-modified borosilicate glasses," Ceram. Int., vol. 51, no. 19, pp. 29344-29353, 2025.

[50] S. S. Chiad, H. A. Noor, O. M. Abdulmunem, and N. F. Habubi, "Optical and structural properties of Ni-doped Co3O4 nanostructure thin films via CSPM," Journal of Physics: Conference Series, vol. 1362, no. 1, 012115, 2019.

[51] Y. S. Song, B. Y. Kim, N. I. Cho, and D. Y. Lee, "Effect of Al doping on optical band gap energy of Al-TiO2 thin films," J. Nanosci. Nanotechnol., vol. 15, no. 7, pp. 5228-5231, 2015.

[52] N. D. M. Said, M. Z. Sahdan, A. Ahmad, I. Senain, A. S. Bakri, S. A. Abdullah, and M. S. Rahim, "Effects of Al doping on structural, morphology, electrical and optical properties of TiO2 thin film," in AIP Conf. Proc., vol. 1788, no. 1, p. 030130, 2017.

[53] A. S. Mohammed and O. A. Fahad, "Sensitivity enhancement for NO2 gas sensor based on Alq3:TiO2," in AIP Conf. Proc., vol. 2372, no. 1, p. 040008, 2021.

[54] Yüce and B. Saruhan, "Al-doped TiO2 semiconductor gas sensor for NO2-detection at elevated temperatures," Tagungsband, pp. 68-71, 2012.

[55] Saruhan, A. Yüce, Y. Gönüllü, and K. Kelm, "Effect of Al doping on NO2 gas sensing of TiO2 at elevated temperatures," Sens. Actuators B Chem., vol. 187, pp. 586-597, 2013.

[56] N. Y. Ahmed, B. A. Bader, M. Y. Slewa, N. F. Habubi, and S. S. Chiad, "Effect of boron on structural, optical characterization of nanostructured Fe2O3 thin films," NeuroQuantology, vol. 18, no. 6, pp. 55-60, 2020.

[57] T. Xie, N. Sullivan, K. Steffens, B. Wen, G. Liu, R. Debnath, and A. Motayed, "UV-assisted room-temperature chemiresistive NO2 sensor based on TiO2 thin film," J. Alloys Compd., vol. 653, pp. 255-259, 2015.

[58] R. Özmenteş and A. S. Hassanien, "Characterizations and optical discussions of thermally evaporated titanium dioxide thin films," Journal of Optics, vol. 54, no. 3, pp. 1322-1340, 2025.

[59] W. Zhao, H. Jia, J. Qu, C. Yang, Y. Wang, J. Zhu, and G. Liu, "Sol-gel synthesis of TiO2-SiO2 hybrid films with tunable refractive index for broadband antireflective coatings covering the visible range," Journal of Sol-Gel Science and Technology, vol. 107, no. 1, pp. 105-121, 2023.